

# **Persistence of a Kelvin-Helmholtz instability complex in the upper troposphere**

M.C. Kelley<sup>1</sup> and C.Y. Chen<sup>2</sup>

School of Electrical and Computer Engineering, Cornell University, Ithaca, NY

R.R. Beland

AFRL, Hanscom Air Force Base, Bedford, MA

R. Woodman and J.L. Chau

Radio Observatorio de Jicamarca, Instituto Geofísico del Perú, Lima, Perú

J. Werne

NorthWest Research Associates, Inc., CoRA Division, Boulder, CO

---

<sup>1</sup> Also at the Department of Earth and Atmospheric Sciences, Cornell University, Ithaca, NY.

<sup>2</sup> Now at Northrop Grumman Norden Systems, Norwalk, CT.

## **Abstract**

During the period of 7-14 September 1998, a multiple instrument campaign was conducted at the Jicamarca Radio Observatory (JRO) near Lima, Peru using a 50 MHz VHF radar and radiosondes. In this paper, we discuss the radar and in situ observations and interpret them with insight gained from high-resolution numerical simulations of the Kelvin-Helmholtz instability (KHI). Evidence is presented that a large-scale shear in the upper troposphere on 8 September 1998 becomes locally unstable due to ambient gravity-wave activity. Isolated KHI events result and subsequently grow and merge to form a large 3 km mixing layer. A 3 km-deep potential-temperature step is observed at the same altitude at least a full day after the initial observations. Analysis indicates that neither turbulent mixing nor radiative cooling is capable of destroying the fully developed temperature step in the 21 hours available, which lends credence to the hypothesis that the structure persisted for this period of time. Alternately, the structure could be continuously generated by a standing wave associated with mountain wave forcing.

## **Introduction**

In September 1998, a campaign called the MIST (Multi-Instrument Stratosphere Troposphere) experiment was conducted in Peru. A combination of remote sensing measurements and in situ observations, coupled with a state-of-the-art numerical simulation, was used to understand the dynamical instability of the upper troposphere. The Jicamarca radar provided remote radar sensing, balloon instrumentation provided the in situ data, and a pseudo-spectral direct numerical simulation (DNS)<sup>3</sup> of the Kelvin-Helmholtz instability (KHI) provided the simulation results.

---

<sup>3</sup> A direct numerical simulation is one that does not attempt to model small-scale turbulent motions, but instead must compute them directly. The primary advantage of this approach is that the solutions are not dependent on unverified turbulence-modeling assumptions. The primary disadvantage is that enormous amounts of computer time and memory are required. See *Werne & Fritts* [1999, 2000, 2001] for details.

This is a rather complete package analogous to prior work by *Klostermeyer and Rüster* [1980, 1981] but with much improved computer capability over the past 25 years.

## **Campaign Description**

The MIST campaign was conducted at the Jicamarca VHF radar site located near Lima, Perú. The radar measurements were conducted from dusk to near midnight each night. Every evening, two or three balloons were launched from the site with a thermosonde system. Below, we briefly describe the radar and thermosonde systems (for more details, see *Chen* [2001]).

The Jicamarca VHF radar (near Lima, Perú) operates at  $\sim 50$  MHz and is a 288 m by 288 m array antenna. The array is composed of 64 modules; each module consists of a 12 by 12 array of cross-polarized half-wave dipoles. During the course of the campaign, three separate radar experiments were performed, two of which involved multi-beam emissions from the radar while the other used only the vertical beam. In this paper we used the data taken during the multi-beam experiments for which the radar was programmed to emit three beams: one pointing nearly vertically, one tilted  $2.5^\circ$  off-vertical pointing to the north, and another tilted at the same angle to the west.

The vertical beam was generated with the whole antenna in one linear polarization so that the two-way full width of the beam at half power is  $\sim 0.8^\circ$ . We generate each oblique beam with two diagonal quarters of the orthogonal polarization. This configuration changes the beam shape from circular to elliptical with a minor axis of  $\sim 0.8^\circ$  in the direction of the tilting and  $\sim 1.5^\circ$  in the orthogonal direction. Since the neutral atmospheric echoes are polarization independent, there is no cross-talk among the signals and the measurements are independent.

The thermosonde system consists of two parts, both of which are mounted below a meteorological balloon. One part is a standard Vaisälä digital GPS microsonde, which makes excellent height-resolution measurements of the standard thermodynamic parameters (pressure, temperature, and humidity) and the horizontal wind velocity (wind speed and direction). The meteorological data are recorded every 1.4 seconds, giving about a 10 m height resolution, and the wind data are recorded every 2 seconds, giving about a 15 m height resolution. The data are carried on the 403 MHz telemetry signal from the radiosonde. A meteorological balloon is used to lift the instrument package with an ascent rate of about 5 m/s.

The second part consists of a turbulence sensor. This sensor measures the root-mean square (RMS) temperature difference between two unheated, fine wire tungsten probes (3.5  $\mu\text{m}$  diameter) separated horizontally by one meter. An analogue instrument performs RMS averaging of the temperature difference. The output of the RMS chip is sampled and transmitted every 1.4 seconds by the radiosonde. The RMS average is computed with a 3.75 second time constant; for a 5 m/s ascent rate, this means an average over 15 m. Finally, the noise floor of the thermosonde corresponds to an RMS temperature difference of 0.002°. The thermosonde system was suspended about 100 m below the balloon to ensure that the turbulent wake from the balloon did not affect the measurements.

## **Data Presentation**

Figure 1 shows three snapshots of the atmosphere over the Jicamarca Radio Observatory (JRO) obtained by balloon-borne instruments on the evening of 8 September 1998. Balloons with the thermosonde system described above were launched at 1830, 2005, and 2143 LT and required ~40 min to reach 13 km. The lower panels show the two wind components while the

top panels show the potential temperature profile. The winds reveal a large-scale shear of  $\sim 3$  km deep and a clear  $\sim 500$  m oscillation that contributes substantially to the local shear rate. At 1830 and 2005 LT, the temperature profiles are characterized by a combination of gradual increases and several sharper steps in the shear flow region. By 2143 LT, the steps seem to be coalescing into two larger steps at around 12 km, each about 1 km deep. The large-scale shear is still strong.<sup>4</sup>

In Figure 2 we show continuous radar data taken on the same day (8 September 1998). From top to bottom, the panels display spectral width from the vertical beam, signal-to-noise (S/N) ratio from the west beam, and the S/N from the vertical beam. Strong signals near and below 9 km are caused by ground clutter from nearby mountains. Development and merging of instability events is best seen in the top panel, which shows the spectral width of the signal. This width is due to turbulent broadening of the signal as turbulence moves the echoing features in the beam range-gate volume (roughly  $300 \text{ m} \times 300 \text{ m} \times 150 \text{ m}$ ). Beam broadening is due to changes in the Doppler shift induced by differences in  $\bar{U} \cdot \tilde{R}$  where  $\bar{U}$  is the background wind and  $\tilde{R}$  is the radar line of sight, which varies within the beam.. This effect is negligible at Jicamarca, given its very narrow beam width [e.g., *Chau et al.*, 2000]. At 1940 LT, the spectral width began to broaden near 11 km and individual layers of  $\sim 500$  m vertical scale are seen to apparently combine into a single layer. Over the next 3.5 hours the turbulent region broadened dramatically, stretching from 9 to 13 km by 2320 LT when the radar time allocation ended.

There is clear evidence for what we believe is the resulting 3 km-deep mixing layer the next day (i.e., 9 September 1998). The balloon soundings for 9 September are presented in Figure 3,

---

<sup>4</sup> We should caution the reader that, because of a non-zero mean wind, the evolution implied by the observations actually results from a combination of temporal evolution and spatial variability of the observed layer as it drifts overhead. Nevertheless, this effect is reduced for the layer reported here because of the fortuitous centering of the layer near the radar site (see Figure 1).

along with the radar S/N for the whole period. We have added a plot of  $C_n^2$ , the refractive index structure function coefficient derived from  $C_T^2$ , the temperature structure function coefficient measured by the balloon-borne probes [Coulman *et al.*, 1995; Walters, 1995]. The dashed line is the measured value and the solid curve is a 300 m boxcar average, which mimics the radar range resolution. Humidity is negligible ( $< 1\%$ ) in the height range where we have good radar data ( $10 \text{ km} < z < 22 \text{ km}$ ). The two arrows indicate strong radar returns from the steep positive gradients in the potential temperature. The temperature step is a solitary feature with the same depth as the radar signature, i.e., 2.4 km. (Remember that the lower part of the radar plot is contaminated by clutter.) Notice also that the shear is significantly reduced.  $C_n^2$  peaks at the edges of the temperature step, consistent with KHI simulations [Werne and Fritts, 1999, 2001; Fritts and Werne 2000] and previous observations [Coulman *et al.*, 1995]. Homogenization of potential temperature in the middle of the layer results from vigorous turbulent mixing there. This concentrates the initial mean potential temperature gradient (and consequently the resulting  $C_n^2$  and  $C_T^2$  peaks) near the edges of the active region.

### Analysis and Interpretation

The gradient Richardson number ( $Ri$ ) for the initial profile on September 8 is plotted in Figure 4, along with the wind speed and potential-temperature profiles from which it was derived.  $Ri$  is defined as  $Ri = N^2 / (dU/dz)^2$  where  $N^2$  is the square of the Brunt-Väisälä frequency and  $dU/dz$  is the shear of the wind magnitude,  $U$ . If one uses the mean gradients apparent in the left two panels for the height range 9-12 km (e.g.,  $d\theta/dz \approx 2 \text{ K/km}$ ,  $dU/dz \approx 0.01 \text{ s}^{-1}$ ),  $Ri$  is estimated to be approximately 0.57. Hence, the large-scale layer is dynamically stable. Note, however, that the right-hand panel reports several nearly periodic excursions below  $Ri=0.25$ , each of which oc-

copy roughly half of the 500 m wavelength evident in the wind profiles. Collectively, these  $Ri$  dips comprise roughly 25% of this height range. We believe these excursions may result from a large amplitude inertial gravity wave that has induced an oscillation in the wind fields and alternately enhanced and weakened the layer stability.

A pseudo-spectral direct numerical simulation (DNS) of the KHI has been performed [Fritts and Werne, 2000; Werne and Fritts, 1999, 2001]. It is relevant to a single wind shear layer, like the seven or eight that are evident in Figure 4(c) before they merge into the large mixing layer shown in Figure 3. Such isolated mixing layers are common throughout the troposphere and stratosphere, but they are more likely to evolve relatively independently of their neighbors (i.e., without multi-layer mergers) in the more stable stratosphere. For this reason we compare the DNS results first with large ( $\delta T$ ) temperature steps observed in the stratosphere during these flights. Figure 5 shows this comparison and demonstrates that the potential temperature profiles for the simulated and observed layers are nearly identical. Other comparisons [Werne and Fritts, 2000] further validate the DNS against atmospheric turbulence measurements (e.g., 2<sup>nd</sup> order structure function constants, spectral slope, and turbulence inner scale), demonstrating the relevance of the simulations to atmospheric turbulence dynamics.

It is noteworthy that, independent of the pathway to the mature state of a well-developed single mixed layer (e.g., through layer merger as in Figure 3 or single KHI evolution as in Figure 5), important aspects of the  $C_n^2$  profiles appear to be universal. For example, the ratio of the  $C_n^2$  peaks at the edges of a mixed layer to the mid-layer value is  $O(10)$  (see Figure 3). This ratio is an important quantity because it describes the source of  $C_n^2$  variability due to wind shear in the atmosphere. The DNS solutions exhibit similar values for this ratio, ranging from 10 to 15 for 50% of the active lifetime of the simulated KH layer.

The time during which the layers are active is markedly different between the simulated and the observed layers. While the simulated layer undergoes restratification and relaminarization after 100 to 130 ( $L/\Delta U$ ) advection time units (here  $L$  is the full layer depth and  $\Delta U$  is the velocity difference across the layer), the observed layer remains well formed 24 hours after layer initiation and exhibits no sign of turbulence subsidence and the consequent restratification. This time span is equivalent to 620 to 1240 ( $L/\Delta U$ ) advection units, where the ambiguity in the time results from the factor-of-two difference in  $\Delta U$  at the beginning and end of the observing period. One possible explanation is that the layer is maintained by continuous forcing of the observed mixing layer by gravity waves, since the simulated KHI amounted to a run-down experiment with a low- $Ri$  initiation but with no subsequent forcing applied to continually feed the dynamics.

Of course, separate from layer forcing is the competing action of layer decay. Several processes can act to limit a mixing layer's longevity, e.g., radiative damping, eddy diffusion, and natural evolution of the stratification and wind-shear environment in which the layer resides. We briefly consider each of these processes below.

First, we investigate infrared radiative damping as a mechanism to damp out the edges of the potential temperature step and bring such a temperature perturbation back to radiative equilibrium. *Fels* [1982] computed the radiative damping time as a function of height, assuming that the vertical wavelength of the temperature perturbation is smaller than the scale height. In the upper troposphere, *Fels* reports a time constant of  $0.05 \text{ day}^{-1}$  for a 300 m-deep layer, so a structure such as we observed clearly can survive for the observed periods against radiative cooling.

Second, we explore eddy diffusion. Using the radar spectral width corrected for beam broadening, peak values of  $\varepsilon \approx 1 \text{ mW/kg}$  are indicated by the September 9 data (not shown). *Bertin et al.* [1997] suggest an eddy diffusivity given by  $D_c = \varepsilon / (3N^2)$ . Using the DNS solutions, we have

verified this expression by evaluating  $D_c \partial \langle T \rangle / \partial z = -\langle \omega \theta \rangle$ , which we found to hold during intermediate and late stages of evolution when the mixing layer is mature. Here  $\partial \langle T \rangle / \partial z$  is the mean temperature gradient,  $-\langle \omega \theta \rangle$  is the eddy heat flux due to turbulent fluctuations, and  $D_c$  is evaluated by computing  $\varepsilon$  exactly, using the numerical solution's velocity derivatives. Using a value of  $\varepsilon = 1$  mW/kg for the observations and  $N^2 = 4.0 \times 10^{-4}$  [rad/sec]<sup>2</sup>, which we deduced from the potential temperature gradient, yields a typical value of  $D_\varepsilon \sim 0.833$  m<sup>2</sup>/s. The edge of the temperature step has a scale length on the order of 300 m. Estimating the lifetime ( $\tau_l$ ) of a turbulent eddy of scale size  $l$  by  $l^2 / D_\varepsilon$ , we find  $\tau_l$  to be about 30 hours.

Finally, we address how we can even discuss such a long time scale when the atmosphere is constantly in motion. Over a 24-hour period at an average velocity of 10 m/s, the air over Jicamarca moves horizontally almost 1000 km. Studies of vertical scattering layers over the Jicamarca Radio Observatory, Peru [Chau *et al.*, 2000] and the Arecibo Observatory, Puerto Rico [Cornish and Larsen, 1989; Cho, 1995] show persistent structures with slow vertical phase velocities. The Arecibo observations were interpreted as inertial period waves with horizontal scales exceeding 3000 km [Cornish and Larsen, 1989; Cho, 1995]. The inertial period at Jicamarca is even longer than over Arecibo, some 58 hours, so very little vertical motion is expected. Therefore, one interpretation is that the persistence of the observed structures is the result of a coherent layer that extends horizontally for thousands of kilometers. An alternate interpretation is that the observed structures are forced by an orographically driven wave field. As such, persistent synoptic scale motions could create a near steady state condition that continues to force a mixing layer. Indeed, the fact that Figure 1 indicates relatively weak initial stratification in the height range of 9-12 km suggests we have witnessed the rejuvenation of a deep fossil mixed layer by an internal wave field. Seemingly, the only way to distinguish between these

competing interpretations is to obtain nearly simultaneous observations over a wide horizontal extent.

**Acknowledgments.** One of the authors (CYC) thanks Dr. Donald Farley for constructive and insightful comments and criticisms. This work was partially supported by the AFOSR through AFRL Lab Task 97PL007 and AFOSR grant F46398-05-5-2005, awarded to Cornell University. JW received support from AFRL contract F19628-02-C-0037. Computer time was made available through a DoD High Performance Computing Modernization Challenge award.

## References

- Bertin, F., J. Barat, and R. Wilson (1997), Energy dissipation rate, eddy diffusivity and Prandtl number: An in situ experimental approach and its consequences on radar estimate of turbulent parameters, *Radio Sci.*, *32*, 791-804.
- Chau, J.L., R.J. Doviak, A. Muschinski, and C.L. Holloway (2000), Tropospheric measurements of turbulence and characteristics of Bragg scatterers using the Jicamarca VHF radar, *Radio Sci.*, *35*, 179-193.
- Chen, C. Y., *A Study of Radar Aspect Sensitivity in the Lower Atmosphere*”, Ph.D. Thesis, Cornell University, Ithaca, NY, 2001.
- Cho, J.Y.N. (1995), Inertio-gravity wave parameter estimation from cross-spectral analysis, *J. Geophys. Res.*, *100*, 18,727-18,737.
- Cornish, C.R., and M.F. Larsen (1989), Observations of low-frequency inertia-gravity waves in the lower stratosphere over Arecibo, *J. Atmos. Sci.*, *46*, 2428-2439.
- Coulman, C.E., J. Vernin, and A. Fuchs (1995), Optical seeing-mechanism of formation of thin turbulent laminae in the atmosphere, *Appl. Opt.*, *34*, 5461-5474.
- Fels, S.B. (1982), A parameterization of scale-dependent radiative damping rates in the middle atmosphere, *J. Atmos. Sci.*, *39*, 1141-1152.
- Fritts, D.C., and J.A. Werne (2000), *Atmospheric Science Across the Stratosphere*, Geophys. Mono. 123, American Geophysical Union.
- Klostermeyer, J., and R. Ruster (1980), Radar observation and model computation of a jet stream-generated Kelvin-Helmholtz instability, *J. Geophys. Res.*, *85*(5), 2841-2846.
- Klostermeyer, J., and R. Ruster (1981), Further study of a jet stream-generated Kelvin-Helmholtz instability, *J. Geophys. Res.*, *86*(7), 6631-6637.

- Walters, D.L. (1995), Measurements of optical turbulence with higher order structure functions, *App. Opt.*, *34*, 1591-1597.
- Werne, J., and D.C. Fritts (1999), Stratified shear turbulence: Evolution and statistics, *Geophys. Res. Lett.*, *26*, 439-442.
- Werne, J., and D.C. Fritts (2000), Structure functions in stratified shear turbulence, DoD HPC User Group Conference, Albuquerque, NM.
- Werne, J., and D.C. Fritts (2001), Anisotropy in a stratified shear layer, *Phys. Chem. Earth*, *26*, 263-268.

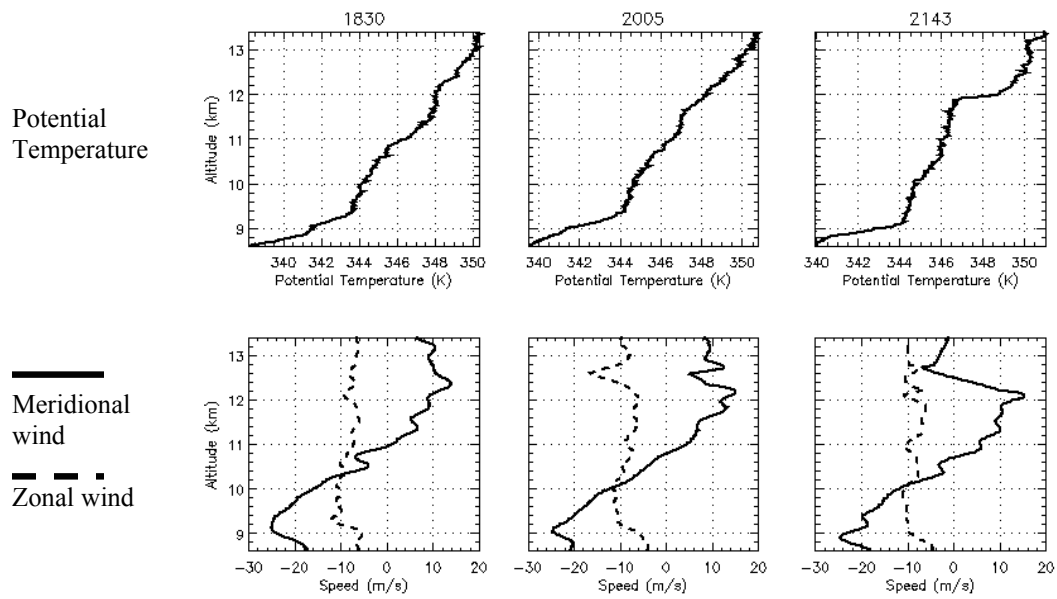


**Figure 1.** In situ measurements made on the evening of 8 September 1998. The lower panels shows the two wind components, while the top panels show the potential temperature profiles. Balloons were launched at 1830, 2005, and 2143 LT.

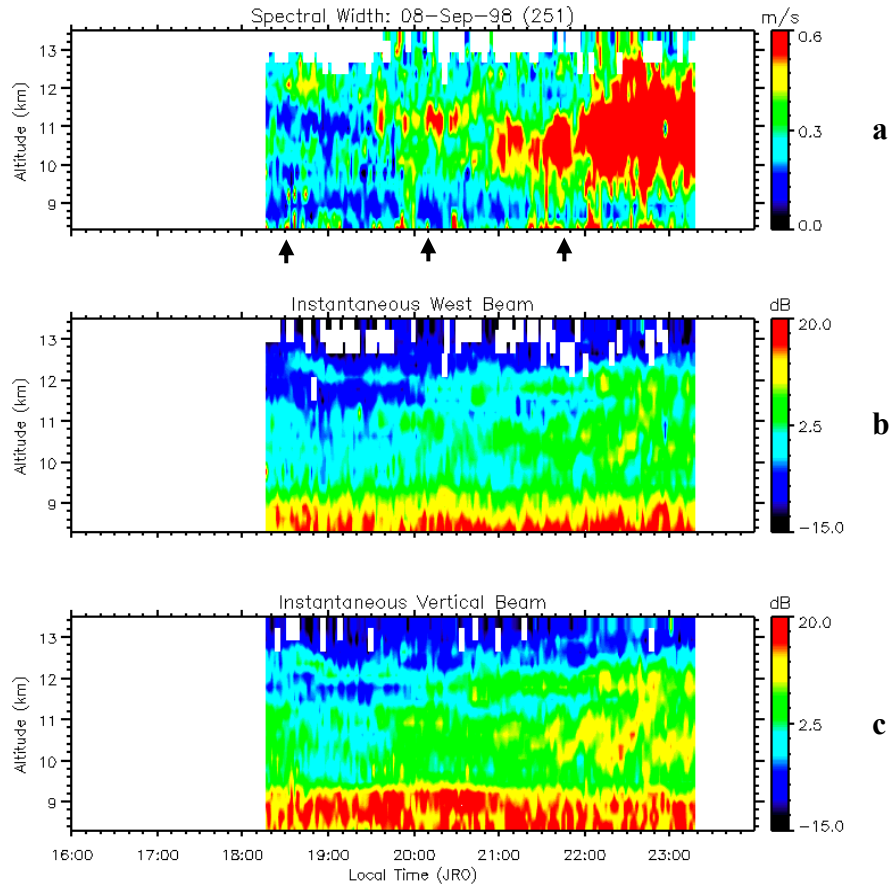


**Figure 2.** Radar measurements taken on 8 September 1998. (a) Spectral width from vertical beam, (b) signal-to-noise (S/N) ratio from the west, and (c) the S/N from the vertical directions. Arrows show when the balloons were launched.

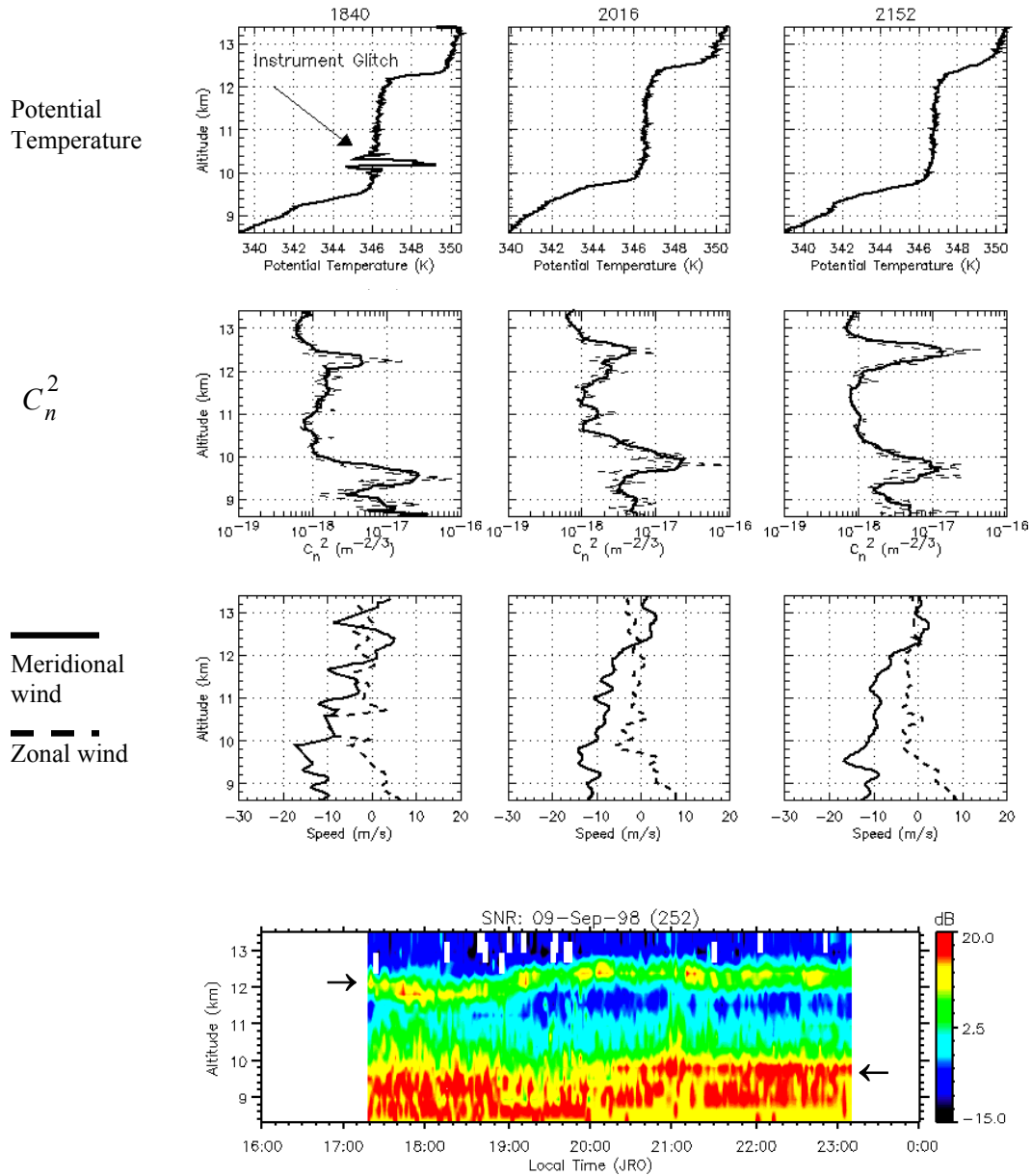


**Figure 3.** Balloon and radar measurements for the evening of 9 September 1998. (a) Potential temperature, (b)  $C_n^2$ , (c) winds, and (d) S/N from vertical beam. Arrows show the strong signals (clutter dominates below 9.3 km).

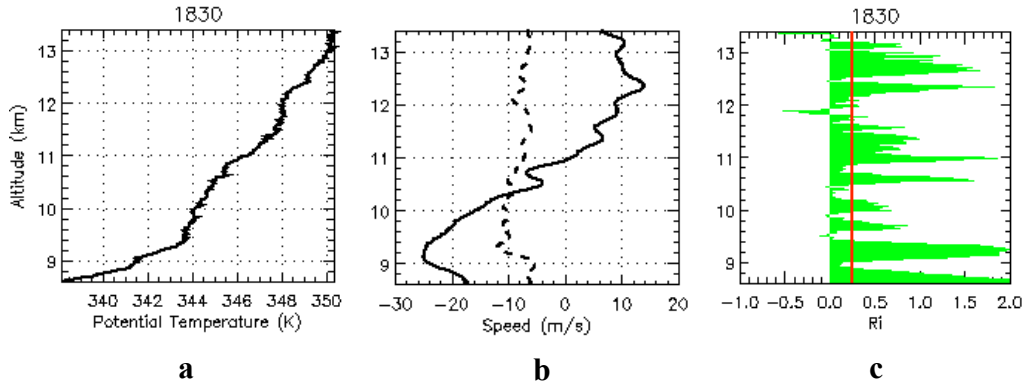


**Figure 4.** In situ measurement made near the altitude of the billow structure on the evening of 8 September 1998: (a) Potential temperature, (b) Meridional wind (solid line) and the zonal wind (dashed line); and (c) Gradient Richardson number ( $Ri$ ). The solid line indicates  $Ri = 0.25$ .

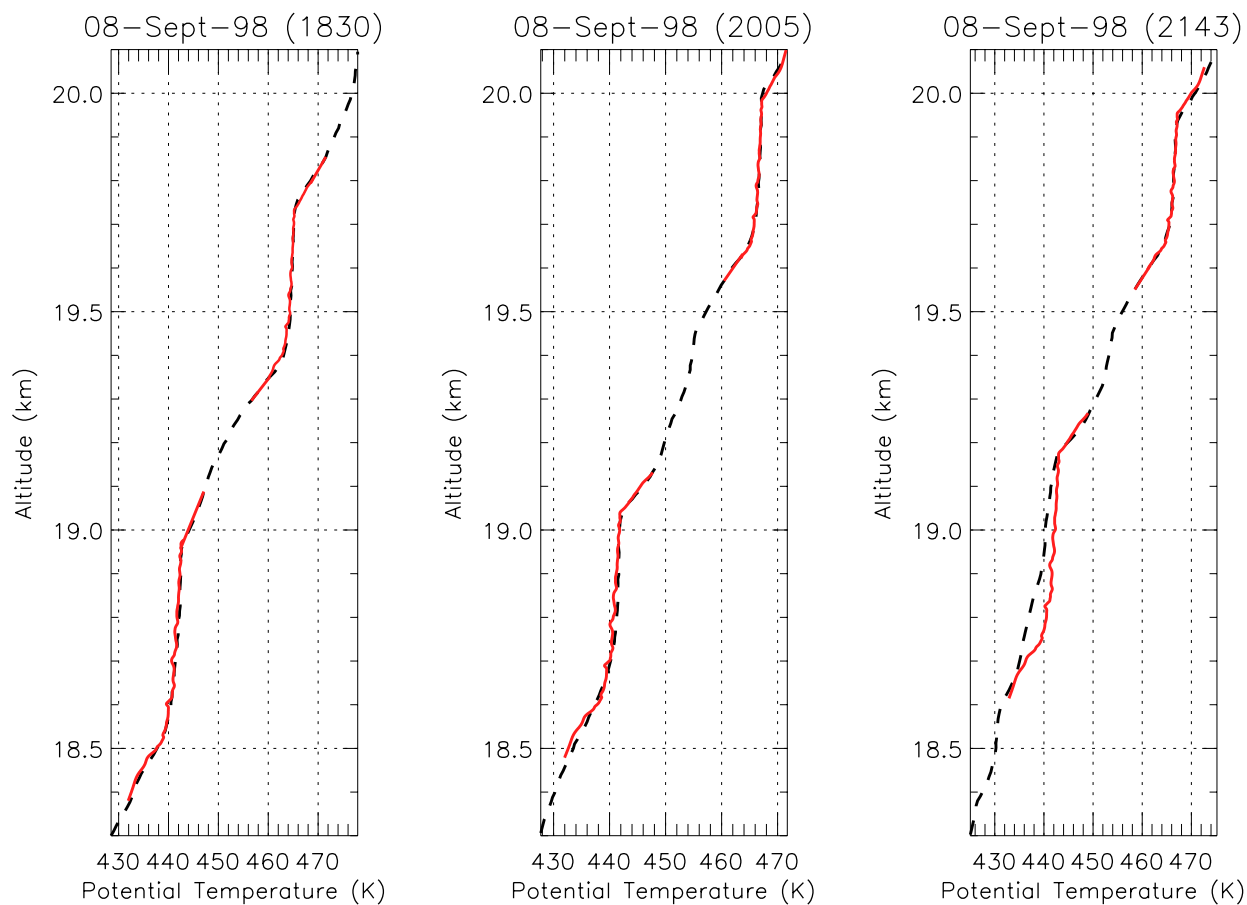


**Figure 5.** Comparison between the balloon-measured potential temperature from 8 September 1998 and potential temperature profiles calculated via the DNS technique. The dashed lines are the measured profiles; the red solid lines are the DNS profiles. The DNS data are averaged horizontally over a region of area  $9\text{ m} \times 9\text{ m}$ , and over  $9\text{ m}$  in the vertical direction.